Monthly Notices
of the
ROYAL ASTRONOMICAL SOCIETY

MNRAS **437,** 2806–2815 (2014)
Advance Access publication 2013 November 30

doi:10.1093/mnras/stt2101

The variable ionized absorber in the Seyfert 2 Mrk 348

E. Marchese,[1]★ V. Braito,[1] J. N. Reeves,[2,3] R. Della Ceca,[4] A. Caccianiga,[4] A. Markowitz,[5,6]† G. Risaliti,[7,8] P. Severgnini[4] and T. J. Turner[3]

[1]*INAF – Osservatorio Astronomico di Brera, via Bianchi 46, I-23807 Merate (LC), Italy*
[2]*Astrophysics Group, School of Physical and Geographical Sciences, Keele University, Keele, Staffordshire ST5 5BG, UK*
[3]*Department of Physics, University of Maryland Baltimore County, 1000 Hilltop Circle, Baltimore, MD 21250, USA*
[4]*INAF – Osservatorio Astronomico di Brera, via Brera 28, I-20121 Milano, Italy*
[5]*Center for Astrophysics and Space Sciences, University of California, San Diego, 9500 Gilman Dr., La Jolla, CA 92093-0424, USA*
[6]*Karl Remeis Sternwarte, Sternwartstrasse 7, D-96049 Bamberg, Germany*
[7]*Harvard–Smithsonian Center for Astrophysics, 60 Garden Street, Cambridge, MA 02138, USA*
[8]*INAF – Osservatorio Astrofisico di Arcetri, Largo E. Fermi 5, I-50125 Firenze, Italy*

Accepted 2013 October 26. Received 2013 October 5

ABSTRACT

We present the results of the analysis of the X-ray spectrum of the Seyfert 2 Mrk 348, observed by *Suzaku* and *XMM–Newton*. The overall spectrum of Mrk 348 can be described by a primary power-law continuum seen through three layers of absorption, of which one is neutral and two are ionized. Comparing *Suzaku* (2008) and *XMM–Newton* (2002) observations we find variability of the X-ray spectral curvature. We suggest that the variability can be explained through the change of column density of both the neutral and one of the ionized absorbers, together with a variation of the ionization level of the same absorber. We thus confirm one of the main features presented in past works, where intrinsic column density variability up to $\sim 10^{23}$ cm^{-2} was observed on time-scales of months. We also find that the photon index of the underlying power-law continuum ($\Gamma \sim 1.8$) is in agreement with the previous observations of this Seyfert 2.

Key words: galaxies: active – galaxies: individual: Mrk 348 – X-rays: galaxies.

1 INTRODUCTION

The extreme energetic phenomena occurring in the nuclei of active galaxies (active galactic nuclei, AGNs) are now recognized to be the result of accretion of large amounts of gas on to a central supermassive black hole, which grows and emits radiation covering a wide range of energies.

In the unified model of AGNs (Antonucci 1993), their different observed properties are explained through orientation effects between our line of sight to the nucleus and 'circumnuclear material'. This circumnuclear gas imprints features – low-energy cut-offs, the Compton hump and emission and absorption lines – on to the primary X-ray emission. However, recent studies have shown that AGNs are more complex than the simple picture of the unified model, where the absorbing matter is uniformly distributed in a toroidal geometry, and located at a pc-scale distance from the central region (Antonucci 1993; Urry & Padovani 1995). In fact, this representation does not fully explain the features observed in all AGNs (Turner et al. 2009; Bianchi, Maiolino & Risaliti 2012; Elvis 2012; Turner, Miller & Tatum 2012); this is the reason why the geometry, size and physical state of the circumnuclear medium of AGNs are still a matter of debate.

Indeed, recent X-ray observations of nearby and bright AGNs showed the co-existence of multiple absorbing components, tracing gas covering a wide range of column densities ($N_{\rm H}$) and ionization states, all of them contributing in giving shape and complexity to the X-ray spectrum we observe (see Turner et al. 2009).

The variability observed in the X-ray spectra of few nearby AGNs showed that this matter is highly structured with a range of ionization states, densities, geometries and locations (Turner et al. 2009; Risaliti 2010) and, in particular, that a significant fraction of the absorbing medium must be clumpy. $N_{\rm H}$ variations have been discovered on various time-scales, allowing one to constrain the location and size of the obscuring clumpy material. There is an increasing number of obscured or type 2 AGNs displaying variability in the X-ray absorbers: NGC 1365 (Risaliti et al. 2005, 2007, 2009; Maiolino et al. 2010), NGC 4388 (Elvis et al. 2004), NGC 7674 (Bianchi et al. 2005), NGC 4151 (Puccetti et al. 2007), NGC 7582 (Xue et al. 1998; Turner et al. 2000; Bianchi et al. 2009), UGC 4203 (Risaliti et al. 2010), Cen A (Rivers, Markowitz & Rothschild 2011), NGC 454 (Marchese et al. 2012) and NGC 4507 (Braito et al. 2013). A few of these sources represent the most extremes cases, known as 'changing-look' AGNs, which show rather strong variability, from

★ E-mail: elena.marchese@brera.inaf.it
† Alexander von Humboldt Fellow.

a Compton-thin state ($N_{\rm H} = 10^{23}\,{\rm cm}^{-2}$) to a Compton-thick state ($N_{\rm H} > 10^{24}\,{\rm cm}^{-2}$), on time-scales from a few days down to a few hours. The short time-scale of some of these occultation events, when detectable, implies that the obscuring clouds are located in the inner region of the AGNs, thus in the proximity of the accretion disc or in the broad-line region (BLR). However, the majority of observations show variations on longer time-scales (of the order of months or year), due either to observational limitations or to the intrinsic nature of the source. Moreover, it is not always straightforward to discern if the X-ray variability is due to a change in the column density of the absorber or to a variation in the primary emission of the X-ray source. Nevertheless, it is now known that the variability of the X-ray absorbers is a common propriety in type 2 AGNs (Risaliti, Elvis & Nicastro 2002) and its analysis can give more information on the structure of the circumnuclear matter.

Mrk 348, as we will discuss below, does not belong to the class of changing-look AGNs, since it was not observed in a state with $N_{\rm H} > 10^{24}\,{\rm cm}^{-2}$; nevertheless, the variability in the absorbing column density along the line of sight allows us to infer that the absorbing material is not homogeneous and stable, but that has to be clumpy. The data discussed here give us information about the geometry, structure and possible location of the absorbers.

Markarian 348 (NGC 262) is a Compton-thin Seyfert 2 galaxy at $z = 0.015$ (Khachikian & Weedman 1974; de Vaucouleurs et al. 1991). The first X-ray observation of this source was performed by *Ginga*, and provided evidence of an absorbed ($N_{\rm H} \sim 10^{23}\,{\rm cm}^{-2}$) X-ray source, with photon index $\Gamma \sim 1.7$ (Warwick et al. 1989). In terms of the unification schemes for Seyfert galaxies, the identification of Mrk 348 as a Seyfert 2 was further confirmed in a work published by Miller & Goodrich (1990) showing that this source is characterized by a broad [full width at half-maximum (FWHM) $\sim$ 7400 km s^{-1}] Hα line component in polarized light. Mrk 348 is a relatively strong radio emitter and was observed by the Very Large Array and the Multi-Element Radio-Linked Interferometer Network (Unger et al. 1984; Antón et al. 2002). It is characterized by a flat radio spectrum continuing well into the infrared, as well as a core-dominated radio structure and rapid radio variability (Neff & de Bruyn 1983). The complex radio properties of this source and the difficulties in determining its orientation with respect to the line of sight make its classification into a radio-quiet or radio-loud source uncertain (Simpson et al. 1996).

Mrk 348 was observed with the *Rossi X-Ray Timing Explorer* (*RXTE*) mission in 12 observations during the period 1996 December 29 to 1997 July 12. Smith, Georgantopoulos & Warwick (2001) analysed these spectra and described the resulting time-averaged 3–20 keV spectrum by a power-law continuum ($\Gamma \sim 1.8$) absorbed by a column density of $N_{\rm H} \sim 10^{23}\,{\rm cm}^{-2}$, plus an FeK$\alpha$ emission line with equivalent width EW $\sim$ 100 eV, plus a Compton reflection component. They found variations in the intrinsic column density occurring over periods of typically weeks to months, with the largest change ($\Delta N_{\rm H} \sim 10^{23}\,{\rm cm}^{-2}$), taking place on a time-scale of $\sim$70 d. They also found X-ray continuum variations with the shortest observed time-scale of $\sim$1 d. Smith et al. (2001) also found that the FeKα line flux did not change significantly during the multiple observations, deducing that much of the line emission is produced in a layer of material with a rather constant sky coverage and thickness, as viewed from the nucleus. They modelled the Compton reflection component using PEXRAV (Magdziarz & Zdziarski 1995), finding that the data were consistent with a reflection strength of $R \sim 0.3$–0.8. The 2–10 keV luminosity measured in these observations was, depending on the $N_{\rm H}$ of each observation, in the range 0.8–3.4 $\times\ 10^{43}$ erg s^{-1} (for $H_0 = 50$; $q_0 = 0.5$), a factor of 3 higher than that measured by *Ginga*.

Smith et al. (2001) suggested that the absorber in Mrk 348 could consist of individual clouds; motions in and out of the line of sight could explain the observed variations in $N_{\rm H}$. Akylas et al. (2002) analysed the same data as Smith et al. (2001) but with additional 25 *RXTE* observations taken in 1996 May–June. This analysis confirmed the spectral variability already observed by Smith et al. (2001). Finally, a more recent work by Singh, Shastri & Risaliti (2011) on the X-ray spectral properties of a sample of Seyfert galaxies analysed the 0.5–10 keV *XMM–Newton* EPIC-pn spectrum of Mrk 348 (2002). They suggested the presence of two absorbers intercepting the primary radiation, a fully covering absorber, with $N_{\rm H} \sim 7 \times 10^{22}\,{\rm cm}^{-2}$, and a partial covering component, with $N_{\rm H} \sim 1 \times 10^{23}\,{\rm cm}^{-2}$ and covering fraction of $C_f \sim 0.84$. They also found a narrow FeKα line with EW $\sim$ 34 eV.

Here we present the results of a *Suzaku* observation (2008 June, net exposure $\sim$76 ks) and the comparison with *XMM–Newton* observation (2002 July, net exposure $\sim$31 ks for EPIC-pn). We show that the spectrum of Mrk 348 can be described by a primary power-law continuum intercepting multiple absorbing components, with different ionization states. We found that the variability of the $N_{\rm H}$ of these layers can explain the observed differences between the *XMM–Newton* and *Suzaku*.

The structure of the paper is the following: in Section 2 we describe *Suzaku* and *XMM–Newton* observations and data reduction; in Section 3 we focus on the modelling of the 0.6–70 keV *Suzaku* spectrum to understand the nature of the X-ray absorption and to evaluate the contribution of the reflection and FeKα emission line on the primary continuum. In Section 4, we compare our *Suzaku* best-fitting model with the *XMM–Newton* spectrum and analyse the variations in some of the best-fitting parameters, i.e. $N_{\rm H}$ and the ionization parameters. Discussion and conclusions follow in Sections 5 and 6. Throughout this paper, a cosmology with $H_0 = 70$ km s^{-1} Mpc^{-1}, $\Omega_\Lambda = 0.73$ and $\Omega_{\rm m} = 0.27$ is adopted.

2 OBSERVATIONS AND DATA REDUCTION

2.1 *Suzaku*

Mrk 348 was observed by the Japanese X-ray satellite *Suzaku* (Mitsuda et al. 2007) on 2008 June 28 for a total exposure time of about 88 ks.

Suzaku carries on board four X-ray Imaging Spectrometers (XIS; Koyama et al. 2007), with X-ray CCDs at their focal plane, and a non-imaging hard X-ray detector (HXD-PIN; Takahashi et al. 2007). At the time of this observation, only three of the XIS were working: one back-illuminated (BI) CCD (XIS1) and two front-illuminated (FI) CCDs (XIS0 and XIS3). All together the XIS and the HXD-PIN cover the 0.5–10 and 12–70 keV bands, respectively. The spatial resolution of the XIS is $\sim$2 arcmin (HEW), while the field of view of the HXD-PIN is 34 arcmin radius. Data from the XIS and HXD-PIN were processed using v2.1.6.14 of the *Suzaku* pipeline and applying the standard screening parameters.[1]

[1] The screening filters all events within the South Atlantic Anomaly (SAA) as well as with an Earth elevation angle (ELV) $<5^\circ$ and Earth day-time elevation angles (DYE_ELV) less than 20°. Furthermore, also data within 256 s of the SAA were excluded from the XIS and within 500 s of the SAA for the HXD. Cut-off rigidity criteria of >8 GV for the HXD data and >6 GV for the XIS were used.

2.1.1 *The* Suzaku *XIS analysis*

The XIS data were selected in 3 × 3 and 5 × 5 edit modes using only good events with grades 0, 2, 3, 4, 6 and filtering the hot and flickering pixels with the script *sisclean*. The XIS response (rmfs) and ancillary response (arfs) files were produced, using the latest calibration files available, with the FTOOLS tasks *xisrmfgen* and *xissimarfgen*, respectively. The net exposure time is 76 ks for each of the XIS. The XIS source spectra were extracted from a circular region of 2.9 arcmin centred on the source, and the background spectra were extracted from two circular regions with radius 2.3 arcmin, offset from the source and the calibration sources. The spectra from the two FI CDDs (XIS 0 and XIS 3) were combined to create a single source spectrum (hereafter XIS-FI), while the BI (the XIS1) spectrum was kept separate and fitted simultaneously. The net 0.5–10 keV count rates are (0.793 ± 0.003), (0.829 ± 0.003) and (0.709 ± 0.003) counts s^{-1} for the XIS0, XIS3 and XIS1, respectively. We considered data in the range 0.6–10 keV for the XIS-FI and in the range 0.6–9 keV for the XIS-BI (ignoring the band 1.6–1.9 keV, due to the presence of instrumental calibration uncertainties). The difference on the upper boundary for the XIS1 spectra is because this CCD is optimized for the soft X-ray band, with higher background at higher energies. The net XIS source spectra were binned at the *Suzaku* energy resolution and then grouped to a minimum of 20 counts per bin in order to use χ^2 statistics.

2.1.2 *The* Suzaku *HXD-PIN analysis*

For the HXD-PIN data reduction and analysis, we followed the latest *Suzaku* data reduction guide (the ABC guide Version 2[2]), and used the rev2 data, which include all four cluster units. The HXD-PIN instrument team provides the background (known as the 'tuned' background) event file, which accounts for the instrumental 'non-X-ray background' (Kokubun et al. 2007). The systematic uncertainty of this 'tuned' background model is ±1.3 per cent (at the 1σ level for a net 20 ks exposure; Fukazawa et al. 2009).

We extracted the source and background spectra using the same common good time interval and corrected the source spectrum for the detector dead time. The net exposure time after screening was 73 ks. We then simulated a spectrum for cosmic X-ray background counts (Boldt 1987; Gruber et al. 1999) and added it to the instrumental one. Mrk 348 was detected at a level of 36.8 per cent above the background.

Fitting this spectrum with a power law, we obtain a photon index $\Gamma = 1.50^{+0.09}_{-0.09}$ and $F_{(14-70\,\mathrm{keV})} \sim 1.5 \times 10^{-10}$ erg cm^{-2} s^{-1}. The extrapolation of this flux in the 14–195 keV band gives $F_{(14-195\,\mathrm{keV})} \sim 3.4 \times 10^{-10}$ erg cm^{-2} s^{-1}. This flux is higher than the *Swift* Burst Alert Telescope (BAT) flux, which is $F_{(14-195\,\mathrm{keV})} \sim 1.6 \times 10^{-10}$ erg cm^{-2} s^{-1}. We also note that *Swift*–BAT observation provides a different photon index, $\Gamma \sim 1.9$, probably due to the wider energy range. If we fit simultaneously *Suzaku* HXD-PIN and *Swift*–BAT spectra, fixing the photon indices to the same value, we find $\Gamma \sim 1.8$; if we extrapolate the flux in the 14–195 keV band for *Suzaku* HXD observation, we find $F^{\mathrm{HXD}}_{14-195\,\mathrm{keV}} \sim 2.3 \times 10^{-10}$ erg cm^{-2} s^{-1}, while the flux measured during *Swift*–BAT observations is $F^{\mathrm{BAT}}_{(14-195\,\mathrm{keV})} \sim 1.6 \times 10^{-10}$ erg cm^{-2} s^{-1}. The variation could be explained by the fact that *Swift*–BAT spectrum is an average of the observations made during 58 months, while HXD observation provides a snapshot of the spectrum, when the flux was possibly higher; therefore, it is not surprising to find intrinsic variations between them.

[2] http://heasarc.gsfc.nasa.gov/docs/suzaku/analysis/abc/

2.2 *XMM–Newton*

XMM–Newton observed Mrk 348 on 2002 July 18 with a total duration of about 50 ks. The *XMM–Newton* observatory (Jansen et al. 2001) carries, among its onboard instruments, three 1500 cm^2 X-ray telescopes, each with EPIC (European Photon Imaging Cameras) imaging spectrometers at the focus. Two of the EPIC use MOS CCDs (Turner et al. 2001) and one uses a pn CCD (Strüder et al. 2001). These CCDs allow observations in the range ∼0.5–10 keV.

During this observation, the pn, MOS1 and MOS2 cameras had the medium filter applied and they were operating in full frame window mode. The data have been processed using the Science Analysis Software (SAS ver. 6.5) and analysed using standard software packages (FTOOLS ver. 6.1). Event files have been filtered for high-background time intervals, and only events corresponding to patterns 0–12 (MOS1, MOS2) and to patterns 0–4 (pn) have been used. The net exposure times at the source position after data cleaning are ∼31.5 ks (pn), ∼38.3 ks (MOS1) and ∼38.2 ks (MOS2). The net count rates in the 0.5–10 keV band are 2.078 ± 0.008 counts s^{-1} (pn), 0.647 ± 0.004 counts s^{-1} (MOS1) and 0.650 ± 0.004 counts s^{-1} (MOS2). The effect of pile-up for this source is negligible.

The results of the analysis of the *XMM–Newton* observation were already published in past works (Guainazzi et al. 2011; Singh et al. 2011), describing a best-fitting model composed of a fully covering absorber ($N_{\mathrm{H}} \sim 7 \times 10^{22}\,\mathrm{cm}^{-2}$), and a partial covering component with $N_{\mathrm{H}} \sim 10.5 \times 10^{22}$ cm^{-2} and covering fraction of $C_f \sim 0.84$. Therefore, for this work we will only use the pn data (the MOS spectra are consistent with it), in order to compare it to the *Suzaku* spectra.

3 SPECTRAL ANALYSIS

All the models were fitted to the data using standard software packages (XSPEC ver. 12.6.0; Arnaud 1996) and including Galactic absorption ($N_{\mathrm{H,Gal}} = 5.86 \times 10^{20}$ cm^{-2}; Kalberla et al. 2005). In the following, unless otherwise stated, fit parameters are quoted in the rest frame of the source at $z = 0.015$ and errors are at the 90 per cent confidence level for one interesting parameter ($\Delta\chi^2 = 2.71$).

3.1 *Suzaku* spectral analysis

For the analysis we fitted simultaneously the *Suzaku* spectra from the XIS-FI (0.6–10 keV), the XIS1 (0.6–9 keV) and HXD-PIN (14–70 keV). We set the cross-normalization factor between the HXD and the XIS-FI spectra to 1.16 (allowing it to vary by ±5 per cent), as recommended for XIS nominal observation processed after 2008 July.[3] The cross-normalization factor between the XIS-FI and the XIS1 spectra was allowed to vary.

As a starting point the data were fitted by a simple model composed of an absorbed primary power-law component and an unabsorbed power law, representing the fraction of primary X-ray radiation that is scattered into our line of sight. The photon indices of these two components were tied to each other. At this first stage we

[3] http://www.astro.isas.jaxa.jp/suzaku/doc/suzakumemo/suzakumemo-2007-11.pdf; http://www.astro.isas.jaxa.jp/suzaku/doc/suzakumemo/suzakumemo-2008-06.pdf

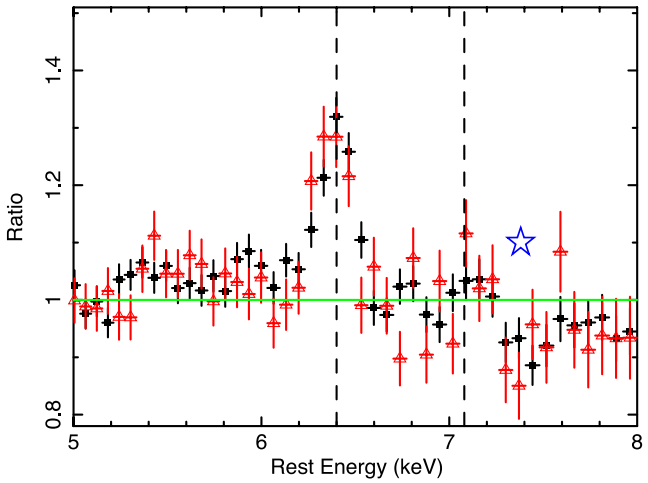

Figure 1. Data/model ratio between the *Suzaku* data (XIS-FI: black filled squares; XIS1: red open triangles) and a basic continuum model composed of an absorbed and an additional unabsorbed (scattered) power law, showing the iron line profile. The two vertical dashed lines correspond to the rest-frame energies of the FeKα and Fe Kβ emission lines at 6.4 and 7.06 keV, respectively. The star indicates a possible absorption feature at ∼7.4 keV.

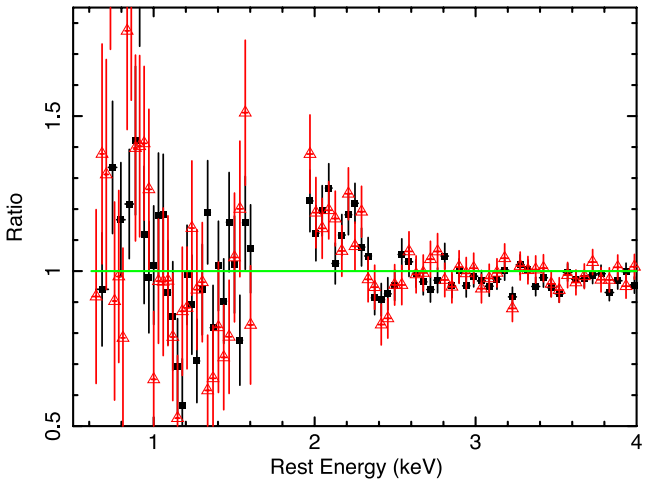

Figure 2. Data/model ratio in the soft X-ray energy region to the *Suzaku* data (XIS-FI: black filled squares; XIS1: red open triangles) and the model including the reflection component (modelled with PEXRAV). These residuals highlight the possible presence of an emission line at ∼2.2 keV and of an absorption line at ∼2.4 keV.

fitted only the continuum, excluding the data between 5 and 7.5 keV where we expected the FeKα emission complex. This model provided a poor fit with a χ^2 of 411.4 for 266 degrees of freedom (d.o.f.), with a photon index $\Gamma \sim 1.57$ and $N_{\rm H} \sim 1.24 \times 10^{23}$ cm^{-2}. When including the data in the 5–7.5 keV energy range, we obtained χ^2/d.o.f. = 950/344. In Fig. 1, we report the residuals of this simple model, including all data, which clearly reveal the presence of emission lines at energies corresponding to the FeKα ($E \sim 6.4$ keV) and Fe Kβ ($E \sim 7.06$ keV) emission lines.

We thus added two Gaussian components, in order to reproduce these emission lines, fixing the energy of the Fe Kβ line to 7.06 keV and its normalization to be 13.5 per cent of the FeKα consistent with the theoretical value (Palmeri et al. 2003). The addition of the FeKα and Fe Kβ lines improved significantly the fit, yielding as an energy centroid for the FeKα line $E = 6.39^{+0.01}_{-0.01}$ keV and for the Fe Kβ line $E = 7.10^{+0.06}_{-0.06}$ keV and a $\Delta\chi^2 = 338.4$ for 3 d.o.f., with respect to the first model applied to all the data (including the 5–7.5 keV energy range). This was still not a good fit (χ^2/d.o.f. = 611.6/341). The equivalent width of the FeKα with respect to the observed continuum is EW $= 81.5^{+9.0}_{-8.8}$ eV, its energy centroid is $E = 6.39^{+0.01}_{-0.01}$ keV and $\sigma = 67.9^{+19.1}_{-21.0}$ eV. Considering that the Compton-thin matter has an $N_{\rm H}$ of $\sim 1.2 \times 10^{23}$ cm^{-2}, we expect it to produce in transmission an equivalent width of EW ∼ 30 eV for solar abundances (Murphy & Yaqoob 2009). Therefore, we can suppose that the measured FeKα equivalent width is mainly due to reflection by Compton-thick matter located out of the line of sight.

Given the presence of a flat continuum ($\Gamma \sim 1.57$) and of the FeKα emission with an equivalent width of EW ∼ 81 eV, we included a Compton reflection component. This component was modelled by adding the PEXRAV model (Magdziarz & Zdziarski 1995). Fitting the model including this component, we obtained χ^2/d.o.f. = 594.0/340 (thus $\Delta\chi^2 = 17.6$ compared to the model with the FeKα and Fe Kβ emission lines). The parameters characterizing the reflected component are an inclination angle i fixed to 60°, abundance $Z = Z_\odot$, a reflection fraction (defined by the subtending solid angle of the reflector $R = \Omega/4\pi$) found to be $R \sim 0.41$ and a normalization fixed to the normalization of the absorbed power law. The fact that the reflection is quite weak is in agreement with the modest equivalent width (EW ∼ 81 eV) found for the FeKα emission line (Ghisellini, Haardt & Matt 1994; Matt, Brandt & Fabian 1996).

The model still did not provide a good fit, in particular between 2 and 2.4 keV, as can be observed in Fig. 2. Thus, we added an emission line at about 2.2 keV and an absorption line at about 2.4 keV, even if we cannot exclude that these features could be instrumental features, such as the Au M edge. This provided a better representation of the soft X-ray spectrum, yielding a χ^2 of 534.1 for 336 d.o.f. ($\Delta\chi^2$ of 59.9 for 4 d.o.f.). The energy centroids found for the lines are $E = 2.22^{+0.02}_{-0.02}$ and $2.42^{-0.03}_{+0.03}$ keV (see Table 1). The model achieved until this point gives the following best-fitting parameters: $\Gamma = 1.75^{+0.06}_{-0.05}$, $R = 0.41^{+0.17}_{-0.16}$, $N_{\rm H} = 1.29^{+0.28}_{-0.31} \times 10^{23}$ cm^{-2}. Since there are still some residuals in the soft X-ray band, we also added a thermal component, modelled through MEKAL (Mewe, Gronenschild & van den Oord 1985) in XSPEC.

We then replaced the neutral reflection component PEXRAV with the PEXMON model (Nandra et al. 2007) in XSPEC, which self-consistently includes the FeKα, Fe Kβ, Ni Kα and the FeKα Compton shoulder. The parameters characterizing PEXMON are

Table 1. Summary of the X-ray emission lines detected for *Suzaku* spectrum in the 2–8 keV energy range. The energies of the lines are quoted in the rest frame. Fluxes and identifications are reported in columns 2 and 3. The EW are reported in column 4 and they are calculated against the total observed continuum at their respective energies. In column 5, the improvement of fit is shown with respect to the continuum model; the value for the model with no lines is χ^2/d.o.f. = 950.0/344.

Energy (keV) (1)	Flux (10^{-6} photons cm^{-2} s^{-1}) (2)	ID (3)	EW (eV) (4)	$\Delta\chi^2$ (5)
$2.22^{+0.02}_{-0.02}$	$8.2^{+1.9}_{-1.9}$	SKα	–	54
$2.42^{+0.03}_{-0.03}$	$-4.6^{+2.4}_{-2.5}$	Sxv	–	22
$6.39^{+0.01}_{-0.01}$	$44.8^{+5.0}_{-4.9}$	FeKα	$81.5^{+9}_{-8.8}$	335
7.06	13.5 per cent FeKα	Fe Kβ	–	5
6.7	<4.8	Fe xxv	<12	0
6.97	<5.8	Fe xxvi	<10	0

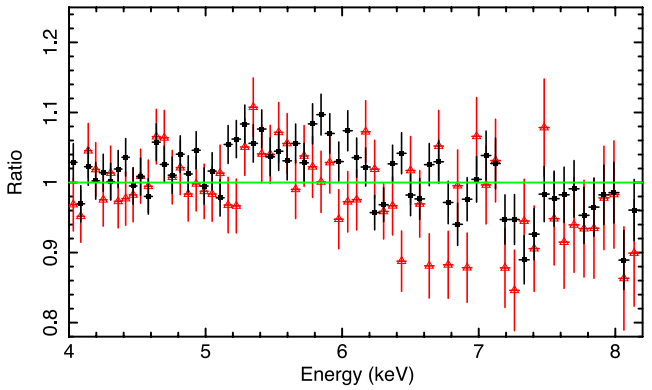

Figure 3. Data/model ratio in the 4–8 keV energy region between the *Suzaku* data (XIS-FI: black filled squares; XIS1: red open triangles) and the model including the reflection component (modelled with PEXMON).

an inclination angle i fixed to 60°, a cut-off energy of $E = 200$ keV (Dadina 2008), a scaling reflection factor R left free to vary, abundance $Z = Z_{\odot}$ and a reflection normalization fixed to the normalization of the absorbed power law. The fit including MEKAL and PEXMON gives a χ^2/d.o.f. = 514.3/337 and $R = 0.43^{+0.04}_{-0.04}$. The fit is still poor due to the presence of residuals in the energy range 5–8 keV (see Fig. 3).

3.1.1 *Fe K complex*

In this section, we discuss the possible presence of emission lines belonging to the Fe K complex and their properties. We looked for signatures of ionized emission lines, by adding a Gaussian component centred at $E = 6.7$ keV and then at $E = 6.96$ keV. The fit did not improve significantly, and the upper limit on the equivalent width of each of these lines is less than 10 eV.

However, if we observe Fig. 3, reporting the residuals of the last model, including the PEXMON component, the presence of a residual weak curvature between 5 and 6 keV and weak absorption lines near 7 keV is noticeable.

First we tested for the presence of broadening of the FeKα emission line, due to relativistic effects manifesting when the line is produced in the inner regions of the accretion disc. Starting from the model including PEXMON, we added a Gaussian component initially centred at about $E = 6.4$ keV, allowing its centroid energy to vary without any constraint. The addition of this component could account for the curvature only through a very broad and not so physical emission line centred at $E \sim 5.6$ keV and with $\sigma \sim 1$ keV. We finally attempted to add a component describing more precisely the line emission from a relativistic accretion disc. Thus, we added the LAOR model in XSPEC (Laor 1991), representing the emission line profile from around a maximally rotating black hole. The outer radius $R_{\rm out}$ was fixed at 100 $R_{\rm g}$, the inclination was constrained to be >45° (appropriate for a type 2 AGN) and we allowed as free parameters the emissivity index, the innermost radius $R_{\rm in}$ and the normalization. The fit still fails to reproduce the curvature, unless the inclination is allowed to vary, reaching a best-fitting value of 25° (χ^2/d.o.f. = 398.7/333), but this produces more than one inconsistency. In fact, it represents a face-on orientation (which is in disagreement with the classification of this source as a Sy2 under classical Sy1/Sy2 unification schemes) and the FeKα line has an equivalent width of EW ∼ 168 eV which, without considering the narrow FeKα emission line, would imply a reflection fraction of $R \sim 1$, in contrast with what we find ($R \sim 0.4$). Given that it appears unlikely to originate from a disc line, we investigated (Section 3.1.2) if the curvature could be due to a more complex absorber.

3.1.2 *Ionized absorber*

Since, as discussed in Section 3.1.1 and shown in Fig. 3, the presence of a weak residual curvature and of weak absorption features is clear, we evaluated if a more complex absorber (i.e. partial covering or ionized) was required by the present data.

First, we included a partial covering absorber in the model, in addition to the fully covering one, resulting in a significant improvement of the fit, yielding $\Delta\chi^2 = 111.9$ for 2 d.o.f. The column density of this absorber is $N_{\rm H} = 1.20^{+5.11}_{-2.65} \times 10^{23}$ cm^{-2} and the covering fraction is $f_{\rm cov} = 0.50^{+0.19}_{-0.14}$. Despite this being a better fit, we note that the curvature in the 5–6 keV region is still present. We then used the best-fitting values obtained by Singh et al. (2011), who adopted the same model, fixing the covering fraction to $f_{\rm cov} = 0.84$ and finding $N_{\rm H,part.cov.} = 9.16^{+0.61}_{-0.67} \times 10^{22}$ cm^{-2} and $N_{\rm H,ful.cov.} = 6.79^{+0.33}_{-0.28} \times 10^{22}$ cm^{-2}. However, the fit gets worse by $\Delta\chi^2 = -11.2$ for 1 d.o.f.

We thus consider if this feature of the spectrum can be better described through an ionized absorber. We added a model representing a photoionized absorber, which is made using a multiplicative grid of an absorption model generated with the XSTAR v 2.1 code (Kallman et al. 2004). This grid describes an ionized absorber parametrized by its turbulence (here we used 5000 km s^{-1}), its $N_{\rm H}$ and its ionization parameter, defined as

$$\xi = \frac{L_{\rm ion}}{nR^2}, \quad (1)$$

where $L_{\rm ion}$ is the ionizing luminosity in erg s^{-1} between 1 and 1000 Rydbergs (13.6 eV to 13.6 keV), n is the hydrogen number density in cm^{-3} and R is the radial distance in cm of the absorber from the ionizing source. The outflow velocity is fixed to zero for simplicity.

We obtained a significant improvement, providing a χ^2/d.o.f. = 385.6/335 ($\Delta\chi^2 = 128.7$ for 2 d.o.f. with respect to the model described at the end of Section 3.1); the parameters obtained with this fit are $N_{\rm H}$ (neutral absorber) $= 5.85^{+0.61}_{-0.66} \times 10^{22}$ cm^{-2}, $N_{\rm H}$ (ionized absorber) $= 1.49^{+0.10}_{-0.09} \times 10^{23}$ cm^{-2} and a photoionization parameter of $\log\xi = 1.83^{+0.15}_{-0.14}$ erg cm s^{-1}. The addition of this mildly ionized absorber succeeds in reproducing the curvature in the 5–6 keV energy range.

Despite being a better description of the data, this model still leaves some residual features in the region 6–7.5 keV, in particular an absorption feature at ∼7.4 keV.

As a first step we added an absorption line, modelled by an inverted Gaussian, with its centroid and width left free to vary. This yielded $\Delta\chi^2 = 7.8$ for 3 d.o.f., with energy of the line $E = 7.40^{+0.07}_{-0.06}$ keV and $\sigma \sim 0.046$ keV, which implies an FWHM of ∼4400 km s^{-1}. Despite that this weak feature is not highly significant, the most likely candidate for it is blueshifted ($v \sim 0.05c$) absorption due to the 1s→2p transition of H-like Fe ($E = 6.97$ keV), while if we assumed a lower ionization state of Fe (i.e. Fe xxv) the corresponding blueshift would be higher ($v \sim 0.1c$).

The last consideration led us to investigate if the weak absorption feature could be well described by substituting the inverted Gaussian component with a second more ionized absorber. At this step, for simplicity, we tied the outflow velocity of the more ionized absorber to the velocity of the mildly ionized one, leaving it free to vary. The resulting fit with this additional component provided χ^2/d.o.f. = 369.3/332 ($\Delta\chi^2 = 16.4$ for 3 d.o.f.), and gives an

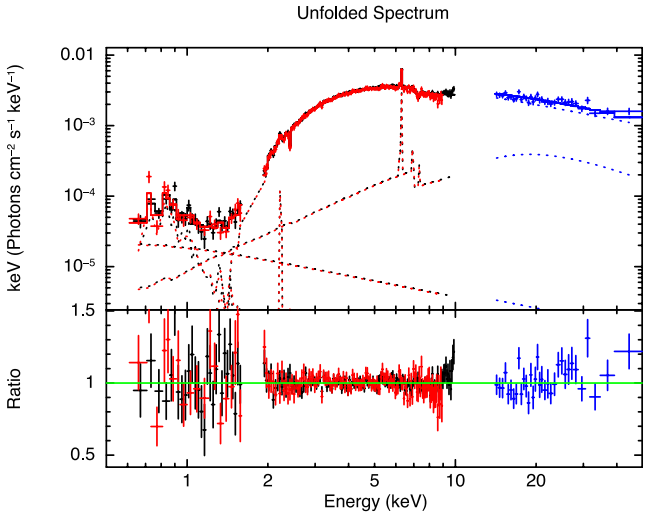

Figure 4. *Suzaku* 0.5–70 keV data and best-fitting model (XIS-FI: black; XIS1: red; HXD: blue) of Mrk 348; data have been rebinned for plotting purposes. The upper panel shows the data and best-fitting model described at the end of Section 3.1.2 (see Table 2 for the best-fitting parameters). The lower panel shows the data/model ratio to this model.

acceptable model for the absorption feature at ∼7.4 keV. Then we tested for an improvement of the fit when leaving free to vary the outflow velocity of the highly ionized absorber. We obtained that the fit did not statistically improve (χ^2/d.o.f. = 364.6/331). The same is true when we fixed the outflow velocity of the more ionized absorber to zero. Thus hereafter we make the simple assumption that the two absorbers have the same outflow velocity.

The model adopted is of the form

$$F(E) = \mathrm{wabs} \times \big[\mathrm{mekal} + (\mathrm{zphabs} \times \mathrm{ion\ abs1} \times \mathrm{ion\ abs2} \times \mathrm{pow1}) + \mathrm{pexmon} + \mathrm{pow2} + 2.2\mathrm{keV\ emis.line} + 2.4\,\mathrm{keV\ abs.line}\big].$$

The main parameters of the best-fitting model are $N_{\mathrm{H\,ion1}} = 1.50^{+0.09}_{-0.09} \times 10^{23}$ cm^{-2}, $N_{\mathrm{Hneutral}} = 4.14^{+0.41}_{-0.40} \times 10^{22}$ cm^{-2}, $N_{\mathrm{Hion2}} = 1.41^{+0.80}_{-0.79} \times 10^{23}$ cm^{-2}, $\log\xi_1 = 1.63^{+0.08}_{-0.07}$ erg cm s^{-1}, $\log\xi_2 = 3.88^{+0.09}_{-0.28}$ erg cm s^{-1} and $v_{\mathrm{ion1,2}} = 0.057^{+0.006}_{-0.005}c$. The best-fit spectrum resulting from this model is shown in Fig. 4. We note that, being the N_{H} of the two ionized absorbers very similar, it could be due to a stratification of the same absorber with different ionization states. This model for *Suzaku* gives a flux in the 2–10 keV energy range of $F_{2-10\,\mathrm{keV}} \sim 3.60 \times 10^{-11}$ erg cm^{-2} s^{-1} and an intrinsic luminosity of $L_{2-10\,\mathrm{keV}} \sim 3.26 \times 10^{43}$ erg s^{-1}.

The value of measured outflow velocity ($0.057c$) is in agreement with assuming an absorption feature due to the blueshifted Fe XXVI absorption line.

Physically this model describes radiation that intercepts a neutral absorber and two photoionized absorbers that have an outflow velocity of ∼$0.06c$, attenuating the primary AGN emission and producing blueshifted absorption lines.

4 *XMM–NEWTON* DATA ANALYSIS

Mrk 348 is a candidate for a variable absorber (Smith et al. 2001; Akylas et al. 2002; Singh et al. 2011). The N_{H} measured with *Suzaku* is a factor of 1.8 lower than the N_{H} reported by Singh et al. (2011) from *XMM–Newton* in agreement with the presence of a variable absorber. Thus, we re-analysed the *XMM–Newton* spectra with some of the models adopted for describing the *Suzaku* spectrum.

We first considered the simplest model, where the reflection is represented by the PEXRAV plus a Gaussian component for the FeKα emission line. When fitting simultaneously the *Suzaku* and *XMM–Newton* data, we found that the energy centroid of the FeKα is consistent between the two observations, while its normalization changed (from $I^{Suzaku}_{\mathrm{Fe\,K}_\alpha} = 4.47^{+0.66}_{-0.65} \times 10^{-5}$ photons cm^{-2} s^{-1} and $\mathrm{EW}^{Suzaku}_{\mathrm{Fe\,K}_\alpha} = 82^{+10}_{-10}$ eV to $I^{XMM}_{\mathrm{Fe\,K}_\alpha} = 2.37^{+0.63}_{-0.61} \times 10^{-5}$ photons cm^{-2} s^{-1} and $\mathrm{EW}^{XMM}_{\mathrm{Fe\,K}_\alpha} = 47^{+13}_{-12}$ eV).

We then adopted the *Suzaku* best-fitting model, where the presence of a reflector plus FeKα and Fe Kβ emission lines was modelled by the PEXMON component. Given the observed variation of the FeKα emission line intensity, we expect that, when applying the best-fitting model simultaneously to *Suzaku* and *XMM–Newton* data, we need different reflection scaling factors of PEXMON.

In order to test the validity of this hypothesis, we investigated the following possible scenarios.

(i) A variable continuum and a constant reflection component, i.e. a scenario in which the reflecting matter is quite far and does not respond immediately to the continuum variability. In terms of fitting parameters, this is represented by

(a) a free normalization of the primary power law between *XMM–Newton* and *Suzaku*;
(b) the reflection parameters of *XMM–Newton* (reflection fraction R and normalization) tied to those of *Suzaku*.

The resulting fit yielded $\chi^2 = 567.7$ for 407 d.o.f., and the assumption of constant reflection leaves residuals in the FeKα region.

(ii) A scenario where both the primary continuum and the reflection component were allowed to vary between *Suzaku* and *XMM–Newton* observations, i.e. a situation where a variability in the continuum reverberates immediately in the reflecting material, which would be located closer in. Thus, the fit was characterized by

(a) a free normalization of the primary power law between *XMM–Newton* and *Suzaku*;
(b) a free reflection fraction R_{XMM} with respect to R_{Suzaku};
(c) the normalization of PEXMON tied to the normalization of the primary power law, for *XMM–Newton* and *Suzaku* independently.

This representation leads to a better fit ($\chi^2 = 551.1$ for 406 d.o.f.), where the continuum is unchanged (variations within the errors) while the reflection fraction does change, as expected.

Thus, we conclude that *Suzaku* and *XMM–Newton* observations do not show continuum variability, but the FeKα emission line does show signs of variation between the two spectra. For this reason, we consider hereafter that a good description is obtained by fixing between *Suzaku* and *XMM–Newton* the continuum and the PEXMON normalizations, while allowing the reflection fraction R to vary freely between the two observations.

In Fig. 5, we plot the *Suzaku* XIS (black, upper spectrum), HXD (blue) and *XMM–Newton* pn (red, lower spectrum) data (using the best-fitting model, see below), confirming a change in the spectral curvature between 1 and 6 keV. We now analyse what are the spectral components that could be responsible for this variation. First of all, we tested the model including the partial covering absorber. Fixing the covering fraction of both *Suzaku* and *XMM–Newton* to $f_{\mathrm{cov}} = 0.84$,

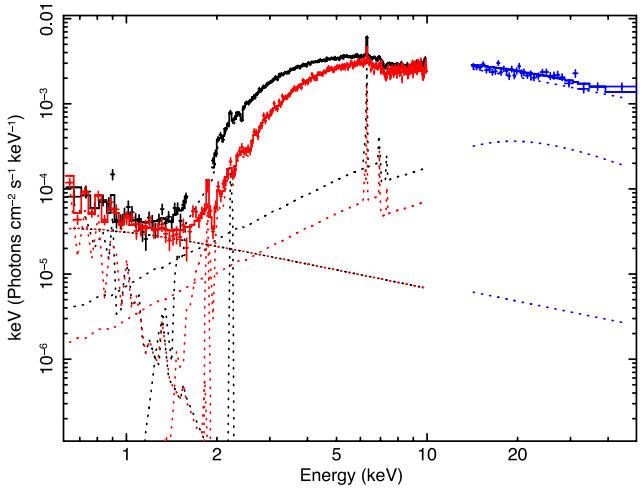

Figure 5. Comparison between the X-ray emission measured with *Suzaku* in 2008 (black data points) and *XMM–Newton* (red data points) in 2002. The continuum model is the best-fitting model composed of a primary power-law component transmitted through a neutral absorber, a scattered power-law component, a Compton reflected component (modelled with PEXMON) and two ionized absorbers.

we obtain that the $N_{\rm H}$ changes from $N^{XMM}_{\rm H\,part.cov.} = 1.55^{+0.12}_{-0.13} \times 10^{23}$ cm^{-2} to $N^{Suzaku}_{\rm H\,part.cov.} = 8.72^{+0.69}_{-0.75} \times 10^{22}$ cm^{-2} for the partial covering absorber, and from $N^{XMM}_{\rm H\,ful.cov.} = 1.16^{+0.05}_{-0.05} \times 10^{23}$ cm^{-2} to $N^{Suzaku}_{\rm H\,ful.cov.} = 6.93^{+0.36}_{-0.31} \times 10^{22}$ cm^{-2}.

Now we consider as a starting point the best-fitting model found for *Suzaku*, thus the model including the ionized absorbers. If we allow as free parameters only the $N_{\rm H}$ of the neutral absorber together with the reflection R factor of PEXMON as well as the soft emission and absorption lines, we find χ^2/d.o.f. = 589.8/409. The neutral absorber column density varies from $N^{Suzaku}_{\rm H\,neutral} = 4.27^{+0.50}_{-0.47} \times 10^{22}$ cm^{-2} to $N^{XMM}_{\rm H\,neutral} = 1.23^{+0.06}_{-0.06} \times 10^{23}$ cm^{-2}.

Since there are some residuals in the 6–8 keV region, we allowed as free parameters the column densities of the ionized absorbers. We obtained χ^2/d.o.f. = 568.7/407 ($\Delta\chi^2 = 21.1$ for 2 d.o.f.); the parameters changing more significantly are the $N_{\rm H}$ of the neutral absorber and the $N_{\rm H}$ of the mildly ionized absorber, implying that the source, when observed with *XMM–Newton*, is generally more absorbed than when observed with *Suzaku*.

We finally allowed also the ionization parameters to vary between *Suzaku* and *XMM–Newton* we obtained χ^2/d.o.f. = 551.6/407. We found similar variations for the $N_{\rm H}$ of the different absorbers, as those mentioned above. The ionization parameter of the mildly ionized absorber changes from $\log\xi_1^{Suzaku} = 1.67^{+0.11}_{-0.10}$ erg cm s^{-1} to $\log\xi_1^{XMM} = 2.04^{+0.19}_{-0.18}$ erg cm s^{-1}. This will be considered as the best-fitting model, and all the relative best-fitting parameters are listed in Table 2.

We note that if we untie the outflow velocity of *XMM–Newton* ionized absorbers with respect to *Suzaku*, we find $\Delta\chi^2 = 17$ with respect to the best-fitting model; the outflow velocity of the first ionized absorber is statistically unchanged, while for the second ionized absorber it is slightly lower ($z = -0.020^{+0.006}_{-0.006}$, corresponding to a velocity of $0.034c$).

We remark that if we attempt to fix the $N_{\rm H\,neutral}$ of *XMM–Newton* to the *Suzaku* best-fitting value, we get a worse fit by a factor $\Delta\chi^2 = 20$.

We conclude that we can account for the difference in the observed X-ray spectra between *Suzaku* and *XMM–Newton* through a variation in absorbing column density of both the neutral absorber and one of the ionized absorbers, together with a change in the ionization parameter of the same ionized absorber.

Table 2. Summary of the *Suzaku* and *XMM–Newton* parameters for the best-fitting models described in Sections 3.1.2 and 4.

Model component	Parameter	*Suzaku* 2006–08	*XMM–Newton* 2002–07
Power law	Γ	$1.72^{+0.02}_{-0.02}$	Fixed to Γ_{Suzaku}
	Normalization[a]	$1.60^{-0.08}_{+0.08} \times 10^{-2}$	Fixed to norm$_{Suzaku}$
Scattered component	Normalization[a]	$3.66^{+0.41}_{-0.42} \times 10^{-5}$	Fixed to norm$_{Suzaku}$
MEKAL	Normalization[a]	$4.34^{+0.71}_{-0.70} \times 10^{-5}$	Fixed to norm$_{Suzaku}$
	$k_{\rm B}T$	$0.24^{+0.02}_{-0.02}$	Fixed to kT_{Suzaku}
Neutral absorber	$N_{\rm H}$	$4.50^{+0.56}_{-0.51} \times 10^{22}$ cm^{-2}	$9.99^{-1.39}_{+1.32} \times 10^{22}$ cm^{-2}
Reflection	R	$0.29^{+0.04}_{-0.04}$	$0.12^{+0.05}_{-0.05}$
Ionized absorber 1	$N_{\rm H}$	$1.44^{+0.10}_{-0.10} \times 10^{23}$cm^{-2}	$2.11^{+0.19}_{-0.18} \times 10^{23}$cm^{-2}
	$\log\xi$	$1.67^{+0.11}_{-0.10}$ erg cm s^{-1}	$2.04^{+0.03}_{-0.01}$ erg cm s^{-1}
	z	Fixed to z of ionized absorber 1	Fixed to z of ionized absorber 1
	$v_{\rm turb}$	5000 km s^{-1}	5000 km s^{-1}
Ionized absorber 2	$N_{\rm H}$	$1.31^{+1.22}_{-0.88} \times 10^{23}$ cm^{-2}	$9.94^{+29.6}_{-0.57} \times 10^{22}$ cm^{-2}
	$\log\xi$	$3.87^{+0.11}_{-0.39}$ erg cm s^{-1}	$3.73^{+0.52}_{-0.27}$ erg cm s^{-1}
	z	$-0.044^{+0.007}_{-0.006}$	Fixed to z_{Suzaku}
	$v_{\rm turb}$	5000 km s^{-1}	5000 km s^{-1}
	$F_{(0.5-2)\,\rm keV}$	$\sim 3.3 \times 10^{-13}$ erg cm^{-2} s^{-1}	$\sim 3.4 \times 10^{-13}$ erg cm^{-2} s^{-1}
	$F_{(2-10)\,\rm keV}$	$\sim 3.6 \times 10^{-11}$ erg cm^{-2} s^{-1}	$\sim 4.2 \times 10^{-11}$ erg cm^{-2} s^{-1}
	$F_{(14-150)\,\rm keV}$	$\sim 7.6 \times 10^{-12}$ erg cm^{-2} s^{-1}	$\sim 7.04 \times 10^{-12}$ erg cm^{-2} s^{-1}
	$L_{(0.5-2)\,\rm keV}$	$\sim 1.72 \times 10^{43}$ erg s^{-1}	$\sim 1.73 \times 10^{43}$ erg s^{-1}
	$L_{(2-10)\,\rm keV}$	$\sim 3.26 \times 10^{43}$ erg s^{-1}	$\sim 3.17 \times 10^{43}$ erg s^{-1}
	$L_{(14-150)\,\rm keV}$	$\sim 4.51 \times 10^{42}$ erg s^{-1}	$\sim 4.20 \times 10^{42}$ erg s^{-1}

[a]Units of photons keV^{-1} cm^{-2} s^{-1}.

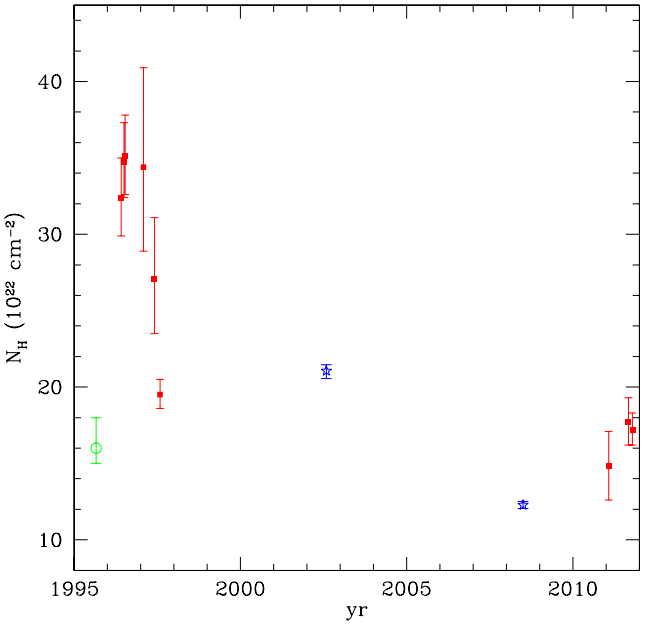

Figure 6. Comparison of the measured values of N_H in *ASCA* observation (Awaki et al. 2000, green empty circles), in *RXTE* observation (red squares) during the time lag from 1997 to 2011 (Akylas et al. 2002 and Markowitz, in preparation for the 2011 data) and the N_H measured from *Suzaku* and *XMM–Newton* observations (blue stars, this work). The N_H values of this work and of *RXTE* observations are based on the abundances relative to solar reported in Wilms, Allen & McCray (2000).

We note that the measured values of N_H found in this work are within the range of the column densities measured in past observations, in particular:

(i) *Ginga* (1987): the measured column density was $N_H \sim 10^{23}$ cm^{-2}.

(ii) *ASCA* (1996 August): as published by Awaki et al. (2000) the column density was $N_H \sim 1.6 \times 10^{23}$ cm^{-2}. We note that during this observation, the observed 2–10 keV flux was $\sim 5 \times 10^{-12}$ erg cm^{-2} s^{-1}, which is, respectively, a factor of 5 and a factor of 7 lower than what we observed with *XMM–Newton* and *Suzaku*. If we hypothesize a scenario where there is a delay in FeKα response with respect to continuum variations, this intrinsic variability in the continuum could be responsible for the different FeKα intensities discussed at the beginning of Section 4. In fact, the lower intensity FeKα line observed with *XMM–Newton* could be responding with a time delay to a different past continuum (in this case a weaker continuum) in a scenario where the reflector producing this emission line is far from the central variable X-ray source.

(iii) *RXTE* (from mid-1996 to mid-1997, and in 2011): N_H took values in the range 0.9–3.2$\times 10^{23}$ cm^{-2} during 14 months between mid-1996 and mid-1997 (Smith et al. 2001; Akylas et al. 2002) and in the range 14–17 $\times 10^{22}$ cm^{-2} during the observation in 2011 (Markowitz et al., in preparation).

We report for clarity in Fig. 6 the measured values of N_H of previous observations together with *XMM–Newton* and *Suzaku* observations.

5 DISCUSSION

The presence of one or more ionized absorbers is not exceptional; indeed, recent sensitive observations with *Chandra*, *XMM–Newton* and *Suzaku* unveiled the presence of red- and blueshifted photoionized absorption lines both in type 1 and type 2 AGNs as well as in radio-quiet and radio-loud AGNs (Tombesi et al. 2010, 2011, 2013; Gofford et al. 2013). Thus, it appears that there is a substantial amount of ionized gas in the nuclei of AGNs, which may be linked to gas outflowing on parsec scales with velocities from hundreds of km s^{-1} up to $v_{out} \sim 0.04$–$0.15c$ (Tombesi et al. 2010, 2012).

It is interesting to make a first-order estimate of the maximum distance of this ionized absorber from the central black hole by means of the equation

$$R_{ion} = \frac{L_{ion} \Delta R}{N_H \xi R} \quad (2)$$

relating the ionization parameter, the density of the absorber and the continuum luminosity L_{ion}. In this case, the estimate of L_{ion} (in the energy range between 13.6 eV and 13.6 keV) from the best-fitting model is of the order of $L_{ion} \sim 7 \times 10^{43}$ erg s^{-1}. Assuming that the thickness of the absorber, $\Delta R = N_H/n$, is smaller than the distance R_{ion} ($\Delta R/R_{ion} < 1$), we can set an upper limit to the distances of each ionized absorber, using *Suzaku* observations:

$$R_{ion} < \frac{L_{ion}}{N_H \xi}. \quad (3)$$

These upper limits are 0.026 and 2.72 pc for the highly and the mildly ionized absorber, respectively. Despite being upper limits, they suggest that the likely location of these absorbers does not correspond to the same radius with respect to the central source. The distance of the first ionized absorber is consistent in being a wind launched from a region located within the BLR.

The higher distance inferred for the mildly ionized absorber is due to the lower ionization parameter, with respect to the highly ionized absorber. Its location could correspond to the region of the molecular torus, at a parsec-scale distance from the central source. However, as this is an upper limit, we should not exclude the possibility that we are observing across this wind; thus, we are not viewing directly the inner radius, which could be located at sub-parsec scales.

Another method to put a constraint on the possible location of these absorbers is to estimate a lower limit on the radial distance by determining the escape radius at which the material will be able to leave the system. This can be determined once we have an estimate of the outflow velocity. Assuming spherical geometry, this radius is

$$R_{esc} \geq \frac{2GM}{v_{out}^2} \simeq \frac{2c^2 R_g}{v_{out}^2}, \quad (4)$$

where R_g is the gravitational radius ($R_g = GM/c^2$). Since the measured outflow velocity is $\sim 0.055c$, we obtain that $R_{esc} \geq 660 R_g$. From the literature, we have estimates of the mass of the central black hole, ranging from $M_{BH} \sim 1.6 \times 10^7$ M$_\odot$ (Woo & Urry 2002) to $M_{BH} \sim 7.5 \times 10^7$ M$_\odot$ (Nikolajuk, Papadakis & Czerny 2004), so we can infer that $R_g \sim 2.5$–11.1×10^{12} cm; thus, $R_{esc} \geq 1.6$–7.3×10^{15} cm ~ 0.0005–0.002 pc. This means that the wind may have been launched at least from a distance of the order of 10^{-4}–10^{-3} pc from the central black hole in order for it to escape, so an origin in the accretion disc or the BLR is plausible. In particular, this estimate suggests that the range of location of the first highly ionized absorber is between 5×10^{-4} and 0.026 pc in the *Suzaku* observation. However, another possibility could be that the wind is part of some aborted outflow, i.e. a wind with outflow velocity lower than the escape velocity and thus unable to leave the system; in that case we would only have an estimate of the maximum distance of the ionized absorber but not the minimum distance from which it was launched.

This analysis highlights the complexity and possible stratifications of the absorbers intercepting our line of sight. Indeed, the observed spectrum could be explained with physically different scenarios: a unique and multiphase absorber, where higher density (and lower ionization) clouds are confined by lower density (higher ionization) clouds, implying that the locations of the two absorbers are actually the same, or a configuration where there are effectively two winds at different physical states and distances, intercepting the line of sight. Neither of these two explanations can be ruled out at the moment, since higher spectral resolution observations are needed.

We conclude that the comparison between *Suzaku* and *XMM–Newton* observations of Mrk 348 does not show extreme variability, such as the transition from a Compton-thick to a Compton-thin state characterizing 'changing-look' AGNs. However, we cannot exclude that, given the long time elapsed between observations, we were not able to observe the source during an obscured Compton-thick phase. We do not observe a variation of the primary continuum, despite past *RXTE* observations which showed brightness variations on time-scales down to 1 d (Smith et al. 2001). The satellite *ASCA* also observed the source (13 years earlier) in a state with flux seven times lower than the flux observed with *Suzaku*.

Mrk 348 can be placed among the large number of AGNs where a non-uniform distribution of the circumnuclear absorbing matter determines $N_{\rm H}$ variations in different epochs. This is consistent with recent theoretical models (Nenkova et al. 2008a,b) and works (Elitzur 2008, 2012) that indicate the possible clumpy nature of the torus, suggesting that the unified model of AGNs is a too simplified scheme. The unified scheme is based on the assumption of a uniform torus, with the same opening angle for all AGNs, implying that the viewing angle is the unique factor determining the classification into type 1 and type 2 AGNs. This is clearly in conflict with both the $N_{\rm H}$ variability and infrared observations (Lutz et al. 2004; Horst et al. 2006) showing that there is no significant difference in the mid-IR emission, normalized to the X-ray flux, of type 1 and type 2 AGNs, contrary to the expectation of strong anisotropy of the unified model. As suggested by Elitzur (2012), these observations are compatible with a 'soft-edged' clumpy torus.

6 CONCLUSIONS

We presented the analysis of the X-ray spectrum of Mrk 348 obtained by *Suzaku* and compared it to the spectrum observed by *XMM–Newton*.

(i) The best-fitting model representing the observed X-ray emission is composed of a primary continuum intercepting three absorbers with different densities and ionizations (including one neutral absorber). We suggest that the location of the neutral absorber and that of the mildly ionized absorber are at a parsec-scale distance, thus consistent with the location of the putative torus. Instead, the highly ionized absorber appears to be located within ∼0.03 pc from the central source, likely in the BLR.

(ii) The comparison with the *XMM–Newton* observation leads to the conclusions that (1) the normalization and photon index of the primary and scattered power law do not vary between the two observations, despite that such variations were observed in past observations (Smith et al. 2001, Awaki et al. 2000); (2) the observed spectral variation requires a change in $N_{\rm H}$ of the neutral ($\Delta N_{\rm H} \sim 5.5 \times 10^{22}$ cm^{-2}) and one of the ionized absorbers ($\Delta N_{\rm H} \sim 6.7 \times 10^{22}$ cm^{-2}).

(iii) We find the presence of the FeKα emission line, with equivalent width EW ∼81 eV during the *Suzaku* observation, in agreement with a fairly weak reflection contribution. During the *XMM–Newton* observation, the equivalent width is lower (EW ∼ 47 eV), and it could be responding to a past weaker continuum, as was observed during earlier *ASCA* observations (Awaki et al. 2000). We do not observe any broadening of the FeKα line as expected for lines produced in the inner regions of the accretion disc, in agreement with the results of Smith et al. (2001) and Netzer, Turner & George (1998).

(iv) We detect a weak absorption line with an energy centroid at $E \sim 7.37$ keV, consistent with a possible blueshifted 1s→2p transition of FeXXVI (at 6.95 keV). We infer that the ionized absorber responsible for this feature has an observed outflow velocity of $v_{\rm out}$ ∼0.05c. Higher resolution observations are needed in order to improve the significance of this detection.

(v) The long time elapsed between the two observations does not allow us to infer the time-scale of the variability, so we can only determine upper limits on the distances of the ionized absorbers. However, as the mass of the central black hole is known from previous works, we can also estimate the minimum escape radius of the outflowing material. The ionization parameters inferred for the two ionized absorbers suggest that one of them must be located at sub-parsec scales, and thus in the region ranging from the accretion disc to the BLR, while the second absorber is likely located at a parsec-scale distance.

ACKNOWLEDGEMENTS

This research has made use of the NASA/IPAC Extragalactic Database (NED) which is operated by the Jet Propulsion Laboratory, California Institute of Technology, under contract with the National Aeronautics and Space Administration. E. Marchese, V. Braito, R. Della Ceca, A. Caccianiga and P. Severgnini acknowledge partial financial support from ASI grants (n. I/023/05/0 and n. I/088/06/).

REFERENCES

Akylas A., Georgantopoulos I., Griffiths R. G., Papadakis I. E., Mastichiadis A., Warwick R. S., Nandra K., Smith D. A., 2002, MNRAS, 332, L23
Antón S., Thean A., Browne I., Pedlar A., in Green R. F., Khachikian E. Ye., Sanders D. B., eds, 2002, ASP Conf. Ser. Vol. 284, IAU Colloq. 184: AGN Surveys. Astron. Soc. Pac., San Francisco, p. 289
Antonucci R., 1993, ARA&A, 31, 473
Arnaud K. A., 1996, in Jacoby G. H., Barnes J., eds, ASP Conf. Ser. Vol. 101, Astronomical Data Analysis Software and Systems V. Astron. Soc. Pac., San Francisco, p. 17
Awaki H., Ueno S., Taniguchi Y., Weaver K. A., 2000, ApJ, 542, 175
Bianchi S., Guainazzi M., Matt G., Chiaberge M., Iwasawa K., Fiore F., Maiolino R., 2005, A&A, 442, 185
Bianchi S., Piconcelli E., Chiaberge M., Bailón E. J., Matt G., Fiore F., 2009, ApJ, 695, 781
Bianchi S., Maiolino R., Risaliti G., 2012, Adv. Astron., 2012, 782030
Boldt E., 1987, Phys. Rep., 146, 215
Braito V., Ballo L., Reeves J. N., Risaliti G., Ptak A., Turner T. J., 2013, MNRAS, 428, 2516
Dadina M., 2008, A&A, 485, 417
de Vaucouleurs G., de Vaucouleurs A., Corwin H., Buta R. J., Paturel G., Fouqu P., 1991, Third Reference Catalogue of Bright Galaxies. Springer, Berlin
Elitzur M., 2008, New Astron. Rev., 52, 274
Elitzur M., 2012, ApJ, 747, L33
Elvis M., 2012, J. Phys.: Conf. Ser., 372, 012032

Elvis M., Risaliti G., Nicastro F., Miller J. M., Fiore F., Puccetti S., 2004, ApJ, 615, L25
Fukazawa Y. et al., 2009, PASJ, 61, 17
Ghisellini G., Haardt F., Matt G., 1994, MNRAS, 267, 743
Gofford J., Reeves J. N., Tombesi F., Braito V., Turner T. J., Miller L., Cappi M., 2013, MNRAS, 430, 60
Gruber D. E., Matteson J. L., Peterson L. E., Jung G. V., 1999, ApJ, 520, 124
Guainazzi M., Bianchi S., de La Calle Pérez I., Dovčiak M., Longinotti A. L., 2011, A&A, 531, A131
Horst H., Smette A., Gandhi P., Duschl W. J., 2006, A&A, 457, L17
Jansen F. et al., 2001, A&A, 365, L1
Kalberla P. M. W., Burton W. B., Hartmann D., Arnal E. M., Bajaja E., Morras R., Pöppel W. G. L., 2005, A&A, 440, 775
Kallman T. R., Palmeri P., Bautista M. A., Mendoza C., Krolik J. H., 2004, ApJS, 155, 675
Khachikian E. Y., Weedman D. W., 1974, ApJ, 192, 581
Kokubun M. et al., 2007, PASJ, 59, 53
Koyama K. et al., 2007, PASJ, 59, 23
Laor A., 1991, ApJ, 376, 90
Lutz D., Maiolino R., Spoon H. W. W., Moorwood A. F. M., 2004, A&A, 418, 465
Magdziarz P., Zdziarski A. A., 1995, MNRAS, 273, 837
Maiolino R. et al., 2010, A&A, 517, A47
Marchese E., Braito V., Della Ceca R., Caccianiga A., Severgnini P., 2012, MNRAS, 421, 1803
Matt G., Brandt W. N., Fabian A. C., 1996, MNRAS, 280, 823
Mewe R., Gronenschild E. H. B. M., van den Oord G. H. J., 1985, A&AS, 62, 197
Miller J. S., Goodrich R. W., 1990, ApJ, 355, 456
Mitsuda K. et al., 2007, PASJ, 59, 1
Murphy K. D., Yaqoob T., 2009, MNRAS, 397, 1549
Nandra K., O'Neill P. M., George I. M., Reeves J. N., 2007, MNRAS, 382, 194
Neff S. G., de Bruyn A. G., 1984, in Fanti R., Kellermann K., Setti G., eds, Proc. IAU Symp. 110, VLBI and Compact Radio Sources. Reidel, Dordrecht, p. 263
Nenkova M., Sirocky M. M., Ivezić Ž., Elitzur M., 2008a, ApJ, 685, 147
Nenkova M., Sirocky M. M., Nikutta R., Ivezić Ž., Elitzur M., 2008b, ApJ, 685, 160
Netzer H., Turner T. J., George I. M., 1998, ApJ, 504, 680
Nikolajuk M., Papadakis I. E., Czerny B., 2004, MNRAS, 350, L26
Palmeri P., Mendoza C., Kallman T. R., Bautista M. A., Meléndez M., 2003, A&A, 410, 359
Puccetti S., Fiore F., Risaliti G., Capalbi M., Elvis M., Nicastro F., 2007, MNRAS, 377, 607
Risaliti G., 2010, in Comastri A., Angelini L., Cappi M., eds, AIP Conf. Ser. Vol. 1248, X-ray Astronomy 2009; Present Status, Multi-Wavelength Approach and Future Perspectives. Am. Inst. Phys., New York, p. 351
Risaliti G., Elvis M., Nicastro F., 2002, ApJ, 571, 234
Risaliti G., Bianchi S., Matt G., Baldi A., Elvis M., Fabbiano G., Zezas A., 2005, ApJ, 630, L129
Risaliti G., Elvis M., Fabbiano G., Baldi A., Zezas A., Salvati M., 2007, ApJ, 659, L111
Risaliti G. et al., 2009, MNRAS, 393, L1
Risaliti G., Elvis M., Bianchi S., Matt G., 2010, MNRAS, 406, L20
Rivers E., Markowitz A., Rothschild R., 2011, ApJ, 742, L29
Simpson C., Mulchaey J. S., Wilson A. S., Ward M. J., Alonso-Herrero A., 1996, ApJ, 457, L19
Singh V., Shastri P., Risaliti G., 2011, A&A, 532, A84
Smith D. A., Georgantopoulos I., Warwick R. S., 2001, ApJ, 550, 635
Strüder L. et al., 2001, A&A, 365, L5
Takahashi T. et al., 2007, PASJ, 59, 35
Tombesi F., Cappi M., Reeves J. N., Palumbo G. G. C., Yaqoob T., Braito V., Dadina M., 2010, A&A, 521, 57
Tombesi F., Cappi M., Reeves J. N., Palumbo G. G. C., Braito V., Dadina M., 2011, ApJ, 742, 44
Tombesi F., Cappi M., Reeves J. N., Nemmen R. S., Braito V., Gaspari M., Reynolds C. S., 2012, in Chartas G., Hamann F., Leighly K. M., eds, ASP Conf. Ser. Vol. 460, AGN Winds in Charleston. Astron. Soc. Pac., San Francisco, p. 8
Tombesi F., Cappi M., Reeves J. N., Nemmen R. S., Braito V., Gaspari M., Reynolds C. S., 2013, MNRAS, 430, 1102
Turner T. J., Miller L., 2009, A&AR, 17, 47
Turner T. J., Perola G. C., Fiore F., Matt G., George I. M., Piro L., Bassani L., 2000, ApJ, 531, 245
Turner M. et al., 2001, A&A, 365, L27
Turner T. J., Miller L., Kraemer S. B., Reeves J. N., Pounds K. A., 2009, ApJ, 698, 99
Turner T. J., Miller L., Tatum M., 2012, AIP Conf. Ser. Vol. 1427, SUZAKU 2011: Exploring the X-ray Universe: Suzaku and Beyond. Am. Inst. Phys., New York, p. 165
Unger S. W., Pedlar A., Neff S. G., de Bruyn A. G., 1984, MNRAS, 209, 15P
Urry C. M., Padovani P., 1995, PASP, 107, 803
Warwick R. S., Koyama K., Inoue H., Takano S., Awaki H., Hoshi R., 1989, PASJ, 41, 739
Wilms J., Allen A., McCray R., 2000, ApJ, 542, 914
Woo J.-H., Urry C. M., 2002, ApJ, 579, 530
Xue S.-J., Otani C., Mihara T., Cappi M., Matsuoka M., 1998, PASJ, 50, 519

This paper has been typeset from a TEX/LATEX file prepared by the author.